

## The X-ray Behavior of Two CVs: TT Ari and DP Leo

Craig R. Robinson and France A. Córdova

*Department of Astronomy and Astrophysics, The Pennsylvania State University, 525 Davey Laboratory, University Park, PA 16802, USA*

**Abstract.** We present ROSAT PSPC observations of the nova-like, or intermediate polar, TT Ari and the eclipsing polar DP Leo. Observations of TT Ari were performed as part of a simultaneous multiwavelength campaign. The X-ray spectrum from the ROSAT PSPC (0.2-2 keV) was combined with Ginga observations (2-37 keV) to suggest the presence of at least three distinct emission components: an optically thin plasma ( $kT_{RS}=0.76_{-0.16}^{+0.20}$  keV), a dominating bremsstrahlung ( $kT_{br}=16.8_{-3.4}^{+4.3}$  keV) continuum and one or more emission lines fit with a single gaussian centered at  $6.57\pm 0.18$  keV. IUE observations show a modulation in the equivalent width of the CIV ( $\lambda 1549$ ) absorption profile on the spectroscopic period indicating a complex wind structure.

The highly variable X-ray light curve of DP Leo exhibits an intensity dip prior to eclipse which has not previously been observed. The dip is interpreted as the eclipse of the main accretion region by an accretion stream varying in shape or impact position on the white dwarf with time. The soft X-ray spectrum is well fit by either a blackbody ( $kT = 24.8_{-8.1}^{+2.6}$  eV) or a soft power law spectrum ( $\alpha \sim 4.0$ ). No evidence exists for accretion onto the stronger magnetic pole and severe limits are placed upon the flux from any hard bremsstrahlung component. A distance upper limit of 500 pc is obtained from the X-ray absorption and a distance estimate of 450 pc was derived through the use of published photometry.

### 1. Introduction

Disk formation occurs in many cataclysmic variables (CVs) and numerous other astrophysical objects from proto-planetary systems to active galactic nuclei. The close proximity, high space density and peak disk luminosity at easily observable wavelengths allow for numerous studies of CV disks and the application of the knowledge gained to models of disks elsewhere in the Universe. However, CVs also provide laboratories for studying the effect on disks of varying mass accretion, tidal forces and magnetic fields. The disruption and distortions of disks and accretion streams in the presence of a magnetic field may be studied through observations of the magnetic CV systems known as intermediate polars (IPs) and polars.

We present ROSAT PSPC observations of a possible IP, TT Ari, and the eclipsing polar DP Leo. The analysis presented here is part of a larger study on the sources and structure of magnetism in CVs.

## 2. TT Arietis

TT Arietis is an unusual CV exhibiting several distinct periodicities in optical photometry, similar to IPs, yet over long time scales it occasionally drops into low states characterized by the “anti-dwarf nova” VY Scl systems (Shafter et al. 1985). The system’s orbital period is observed from radial velocity measurements of emission lines to be 0.13755114(13) d (Thorstensen et al. 1985) while the photometric period is shorter with a value around 0.1329 d (see Tremko 1992). This binary was found to be a hard X-ray source using the Einstein X-ray satellite (Córdova, Mason & Nelson 1981). The Einstein data are consistent with modulations of the X-ray flux with either the spectroscopic or photometric periods (Jensen et al. 1983) while EXOSAT data exhibit no conclusive evidence for strictly periodic modulations (Hudec et al. 1987). A 4 day periodicity found in U-band photometry (Semeniuk et al. 1987) suggests the presence of variations at the beat period between the spectroscopic period ( $\sim 3.3$  hr) and the photometric period ( $\sim 3.2$  hr). This behavior is similar to the intermediate polar TV Col where the spectroscopic period ( $\sim 5.5$  hr) is slightly larger than the photometric period ( $\sim 5.2$  hr) and a variation at the 4 day beat period is observed (Hellier et al. 1991).

The TT Ari observations presented here are part of a simultaneous multiwavelength campaign combining observations from ROSAT, IUE, Ginga and several ground-based observatories. Future papers will explore the observations across all of these wavelengths. The ROSAT PSPC observations of TT Ari occurred 1991 August 1.3 to 2.2 for a total of approximately 25 ksec of usable data. Ginga and IUE observations were obtained over part of the ROSAT observations. The background subtracted PSPC count rate was  $0.42 \pm 0.01$  cts  $s^{-1}$ .

Spectral models were fit simultaneously to the ROSAT and Ginga data sets. These observations are described more fully within Robinson, Córdova & Ishida (1993). Figure 1 shows the photon spectrum resulting from the best fit model together with the observations. The spectrum is dominated by a thermal bremsstrahlung continuum characterized by a temperature of  $kT = 16.8_{-3.4}^{+4.3}$  keV. An additional component was modeled as a Raymond-Smith plasma of temperature  $0.76_{-0.16}^{+0.20}$  keV. The derived absorption column density was determined to be  $N_H = 4.4 \pm 0.5 \times 10^{20}$   $cm^{-2}$ . An emission line centered at  $6.57 \pm 0.18$  keV, with an assumed line width ( $\sigma$ ) of 0.1 keV and resulting equivalent width of 0.89 keV, was added to the other components. A strong iron ( $K\alpha$ ?) emission line was suggested by Ishida (1991) in the Ginga spectra of all observed polars and IPs. Other iron lines may exist but cannot be distinguished by Ginga.

The resulting unabsorbed X-ray luminosity in the observed energy range is  $L_x(0.2-37.4 \text{ keV}) = 1.4 \times 10^{32}$   $erg \text{ s}^{-1}$  assuming an estimated lower limit distance of 200 pc (Shafter et al. 1985). The observations of TT Ari suggest that neither ROSAT nor Ginga alone provided enough information to adequately model its X-ray spectrum. Fits to Ginga data produce no evidence of the softer component and over-estimate the absorption while ROSAT data alone places only limited constraints on the bremsstrahlung continuum. The energy range covered by ASCA, together with its spectral resolution capabilities should greatly improve our understanding of the multiple X-ray emission components in TT Ari and similar systems.

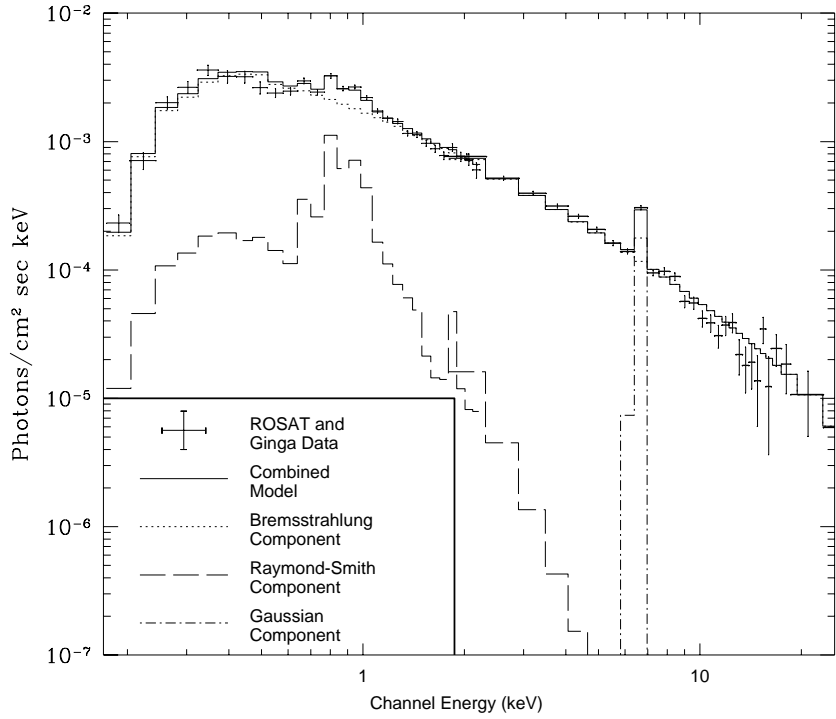


Figure 1. The Ginga and ROSAT X-ray spectra of TT Ari.

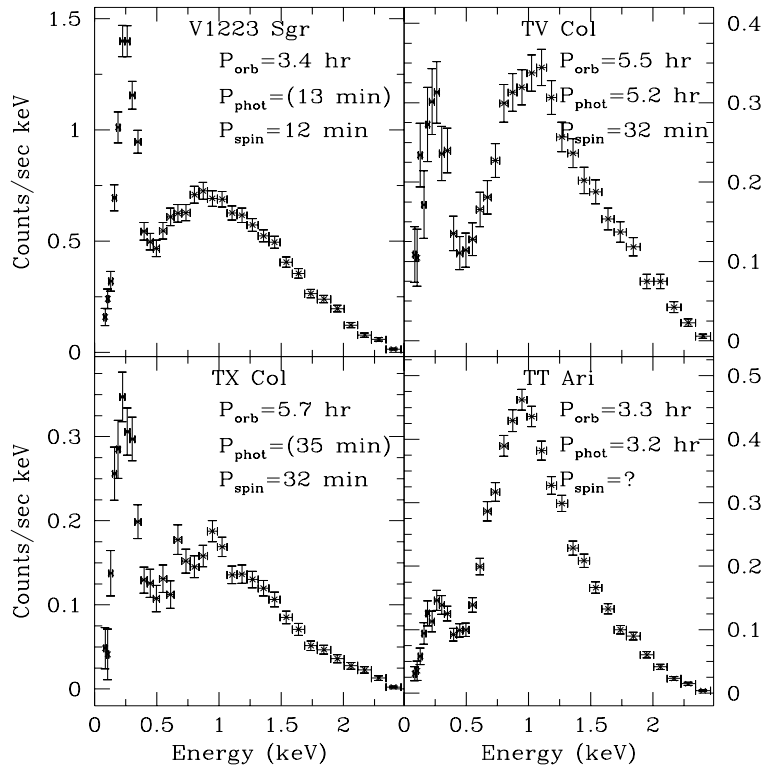


Figure 2. ROSAT count spectra of 3 IPs and TT Ari.

After years of observations, the physical mechanisms producing variations in various spectral bands for TT Ari are still not understood. We began our analysis of the X-ray data by comparing the observations of TT Ari to similar systems. Therefore, in Figure 2 we show the count spectra of TT Ari and three IPs exhibiting some similar characteristics. The general shapes of the count spectra are governed by the response of the PSPC. The systems TV Col and TX Col have similar orbital and spin periods, but TV Col exhibits an optical photometric period slightly shorter than its orbital period and TX Col shows photometric variations at the beat period between orbital and spin periods. TT Ari and V1223 Sgr have similar orbital periods but V1223 Sgr has a clearly defined spin period and photometric variations at the beat frequency. Initial spectral modeling of the three IPs suggests a larger absorption column density exists for these three objects than for the harder spectral source TT Ari. The IP spectra appear to require multiple emission components for fits to their spectra with fits in TV Col and TX Col suggesting a combined soft optically thin plasma and harder bremsstrahlung continuum.

X-ray flares were detected in the simultaneous ROSAT and Ginga data sets but were not found to be strictly periodic. Simultaneous optical and X-ray flares were also observed and analysis of the combined data sets continue. Archival IUE data were extracted from observations obtained by C. Mansperger during a portion of the simultaneous campaign and observations by Verbundt 47 days later. Variability in the CIV ( $\lambda 1549$ ) line of TT Ari was first reported by Guinan & Sion (1980) who showed that this line exhibits a P Cygni profile with great variability in both the absorption and the emission components. A plot of equivalent width against spectroscopic phase for the 1991 data (using the Thorstensen et al. (1985) ephemeris) is shown in Figure 3. The absorption component appears modulated on the spectroscopic period with maximum absorption occurring near 0.8 phase. Analysis of the variations on the reported photometric periods do not show such a relationship. The 47 day time span between the two IUE data sets significantly offsets the photometric and spectroscopic phases to enable us to distinguish between variations on these different periods. The orbital variability in the CIV absorption may be due to an asymmetric wind arising from the disk or regions on the white dwarf. However, the variations in the emission component appear more complex and may be inde-

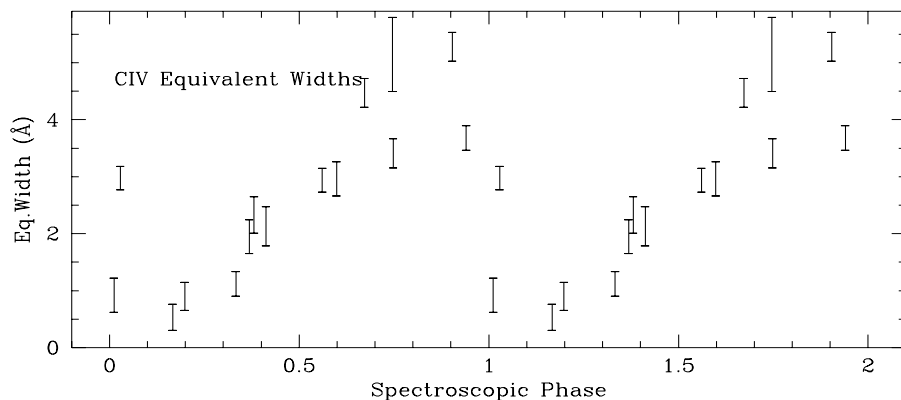


Figure 3. TT Ari equivalent widths from CIV absorption.

pendent of the source of absorption component variability. We are currently studying the relationship between flaring events in X-rays and the variations observed with IUE.

### 3. DP Leonis

The eclipsing magnetic binary DP Leo belongs to the class of CVs known as polars. AM Her binaries, or polars, contain a synchronously rotating white dwarf with a sufficiently high magnetic field to disrupt the formation of a disk by material accreting from its low mass companion. These systems, reviewed recently by Cropper (1990) and Voikhanskaya (1990), and within the CV review of Córdova (1993), exhibit cyclotron emission in the optical and IR, soft X-ray quasi-blackbody emission ( $kT \sim$  tens of eV), and a hard X-ray bremsstrahlung spectrum ( $kT \sim$  tens of keV) with strong iron emission lines superimposed. An accretion stream, accelerated to supersonic speed, moves along the magnetic field lines of the white dwarf toward one (or more) of the magnetic poles where a shock region, near to the surface, is formed. Heated to tens of keV, the post-shock matter cools through bremsstrahlung emission, while electrons spiraling in the magnetic field (tens of MG) produce the observed cyclotron emission. Reprocessing of the hard X-ray photons in the stellar atmosphere of the white dwarf and/or large blob accretion in the white dwarf’s photosphere produce the softer X-ray component visible in all polars. The ratio of the hard to soft X-ray fluxes in these systems provides important clues in determining the sources of these X-rays.

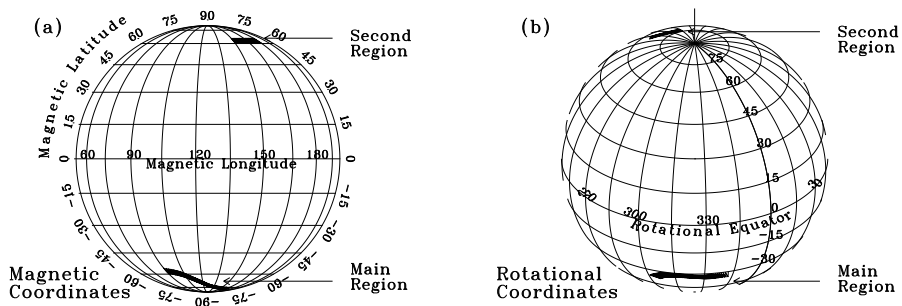


Figure 4. Projections of the cyclotron emission regions for DP Leo as determined by CW in (a) magnetic coordinates and (b) rotational coordinates. Photometric modeling suggests that these cyclotron regions and EINSTEIN observed X-ray emitting regions may be coincident. These diagrams correct the inconsistent longitude scale within CW.

Recent photometric observations by Bailey et al. (1993, hereafter BWF) suggest that the longitude of the accretion stream impact spot in DP Leo has changed from  $-14^\circ \pm 4^\circ$  (1984) to  $+4^\circ \pm 3^\circ$  (1992), where a positive accretion spot longitude implies that the spot leads the secondary component. A similar behavior of a variable accretion spot position relative to the line of centers between the two components was also shown to occur in another polar, WW Hor,

but the variations occurred in the opposite direction in longitude. This opposite behavior together with a clustering of accretion spot longitudes in polars near  $+20^\circ$  led BWF to conclude that non-synchronous rotation of the white dwarf, which would not produce such a skewed distribution, is an unlikely explanation for the observed accretion spot longitudinal drifts.

The modeling, in DP Leo, of a strong cyclotron hump in phase resolved spectra by Cropper & Wickramasinghe (1993, hereafter CW) has shown two cyclotron emitting regions exist. The main emitting pole is modeled by CW using a field of 30 MG and is located between  $30^\circ$  and  $40^\circ$  below the rotational equator, trailing slightly the line of centers of the two stars. The second emission region has a magnetic field strength of 59 MG, nearly twice that of the main pole, and is positioned near the upper rotational pole but nearly opposite to the secondary star (see Figure 4). The differing magnetic field strengths of the two poles and their angular separation of significantly less than  $180^\circ$  implies a magnetic field configuration significantly more complex than a centered dipole. Wu & Wickramasinghe (1993) suggest a combination dipole-multipole model for polars where the white dwarf’s main pole oscillates with respect to the secondary.

ROSAT PSPC observations were obtained of DP Leo during four intervals between 1992 May 30 and June 1 totaling 8910 seconds. The observation intervals covered three eclipses of the X-ray emitting region by the secondary. The orbital period of DP Leo ( $\sim 89$  min.) is slightly shorter than the orbital period of the ROSAT spacecraft which allowed for the observation of the last two eclipses to be consecutive while the first eclipse was observed one day earlier. Photons detected within the acceptable time windows were extracted from a circular region centered on DP Leo with a radius of 3.5 arcminutes. Five nearby regions, each with the same radius as the source region and apparently free of sources, were used to determine the background level. The background subtracted source count rate was  $0.27 \pm 0.01$  cts  $s^{-1}$  over the entire observation and  $0.34 \pm 0.01$  cts  $s^{-1}$  within 0.3 phase of the eclipse (the “bright phase”).

The spectral analysis was performed using the “DRM 36” response matrix which is the appropriate choice for AO2 observations (Turner & George 1993). The background subtracted source spectrum was binned from 256 energy channels into the SASS standard 34 energy channels. The highest two energy channels were excluded from further analysis due to uncertainties in the detector response. The lowest 4 out of the 34 energy channels are known to be problematic due to the incorrect position determination of some low energy X-ray photons producing “electronic ghost images” (Nousek & Lesser 1993). The effect of the soft energy halo created by these ghost images is greatest in the first two energy channels and was expected to be minimized in our analysis by extracting the source using a large radius (3.5 arcminutes). However, a large drift in the energy to PI channel transformation, calibrated at 1.49 keV, appears to have caused a deficit of photons in the lowest two energy channels (Turner & George 1993). This effect is seen in the ROSAT spectrum of DP Leo (Figure 5) where the steep initial increase in the spectrum, visible in the first 3 channels, is larger than is plausible for the energy resolution of the PSPC detector. Therefore, while the DP Leo spectrum is quite soft with no significant detection of source photons in energy channels 12 or above ( $E > 0.47$  keV), we determined it necessary to exclude the first 2 energy channels from spectral fits.

The soft X-ray component in the spectra of polars is thought to arise from either large accretion column blobs which permeate the shock region above the white dwarf and reach the photosphere where they cool through thermalized soft X-rays, or through the reprocessing of hard X-ray bremsstrahlung emission, produced in the post-shock region, and cyclotron radiation, generated by free electrons flowing along the magnetic field lines (Frank et al. 1988). The existence of a hard X-ray component in DP Leo cannot be confirmed in the ROSAT data.

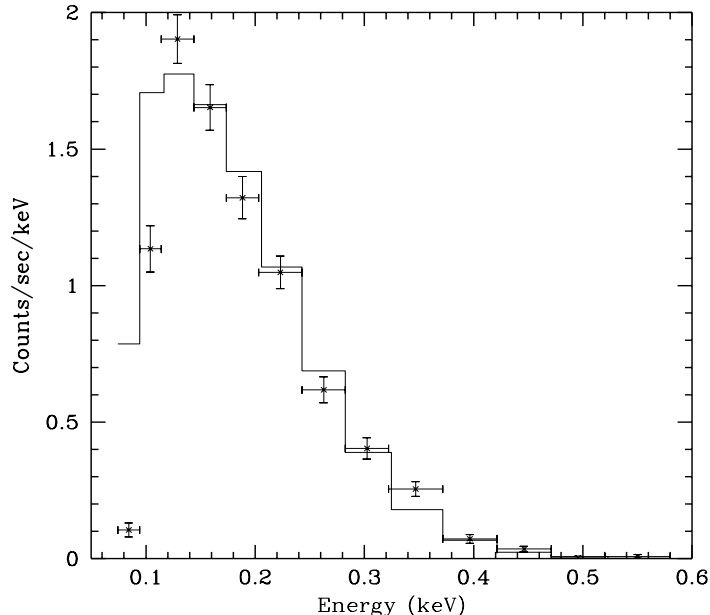


Figure 5. ROSAT spectrum of DP Leo with blackbody fit. The first two channels were not used in determining this fit (see text).

During the 1992 ROSAT observations, 99 counts were detected in the source region, above 0.47 keV, compared with a corresponding background of  $74.8 \pm 10.1$  counts. An upper limit to the source intensity contributing the observed counts was calculated following the Bayesian statistical method and assuming a constant prior (Kraft, Burrows & Nousek 1991). The 90% confidence interval upper bound is 41.3 counts resulting in a count rate of  $4.64 \times 10^{-3}$  cts  $s^{-1}$  attributable to the source.

The observed soft spectrum was fitted using single component models with absorption. Acceptable fits were obtained both with a power law and with a blackbody component. However, physical models predict blackbody-like emission to occur. For the power law model, the best fit was found using an unabsorbed power law with spectral index,  $\alpha$ , of 4.0. The resulting  $\chi^2$  statistic for this model was 23.5 (28 d.o.f). The blackbody model exhibited a best fit,  $\chi^2 = 25.3$  (28 d.o.f), where again the source was unabsorbed with a temperature of  $kT = 24.8_{-5.4}^{+1.9}$  eV (see Figure 5). The calculation of 90% confidence intervals limits the absorption column density to  $N_H < 5 \times 10^{19}$   $cm^{-2}$  and allows for blackbody temperatures between 19.4 and 26.7 eV (see Figure 6).

EINSTEIN observatory observations of DP Leo from 1979 (see Biermann et al. 1985) were extracted and a spectral fit was performed to the data. The

spectral models were not well constrained due to the low sensitivity of EINSTEIN at soft energies. However, the data were consistent with the ROSAT spectral fits and a harder component was not found. EXOSAT observations of DP Leo were obtained in 1984 with a firm detection in the low energy (LE) detector using the thin lexan filter but no source was detected using the aluminum/parylene filter or with the medium energy (ME) instrument (Schaaf et al. 1987).

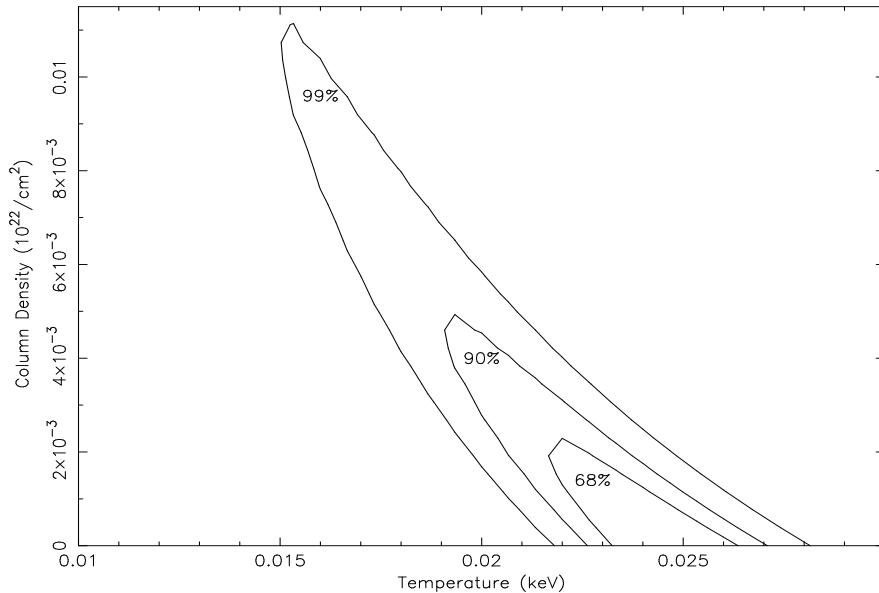


Figure 6. ROSAT blackbody fit confidence contours.

A lower distance limit of 380 pc was previously determined by Biermann et al. (1985) based upon their mass estimate for the secondary of around  $0.098 M_{\odot}$  and their non-detection of the secondary to an R-magnitude of 22. A measurement of the R-magnitude of the secondary and its mass was recently performed by BWF from a fit to their photometric light curve. They obtained a solution with a mass of  $0.106 M_{\odot}$  for the secondary and an R-magnitude of 21.8. Based upon the work of Young & Schneider (1981), the absolute R-magnitude of such a star should be around 13.54. The system has little absorption resulting in a distance estimate of 450 pc.

An independent upper limit to the distance is obtained from the X-ray spectral fit. The DP Leo system is located in a region of unusually low density. The distance could be as far as approximately 500 pc, based upon the observations of this region by Frisch & York 1983, while still exhibiting a column density  $< 5 \times 10^{19} \text{ cm}^{-2}$  (the upper limit in the 90% confidence contour). The derived blackbody spectral fit together with the calculated distances, when combined with the appropriate geometrical corrections based upon viewing angle, yield an upper limit to the source luminosity of  $L_x(0.1 - 0.5 \text{ keV}) = 6.0 \times 10^{31} \text{ erg s}^{-1}$  for a distance of 500 pc and an estimate of  $L_x(0.1 - 0.5 \text{ keV}) = 4.8 \times 10^{31} \text{ erg s}^{-1}$  for a distance of 450 pc.

The X-ray light curve from the PSPC, derived using all 34 energy channels, is presented in the top plot of Figure 7 for the entire data set and the lower plots for each of the individual eclipses. The phase was computed using the



ephemeris of Schmidt (1988):  $\text{HJD}2444214.55283(17) + 0.062362849(6)\text{E}$ . The data are binned into 200 equally sized bins of length 26.94 seconds each. Two dips are visible in the light curves with the first dip centered near phase 0.943. The second dip, centered slightly before 1.0 phase, is suspected of being the previously observed eclipse of the X-ray emitting region on the white dwarf by the secondary companion. No evidence exists for accretion onto the second pole, as was suggested by EXOSAT observations from 1984 (Schaaf et al. 1987) and by cyclotron humps in phased resolved spectra from 1988-89 (CW).

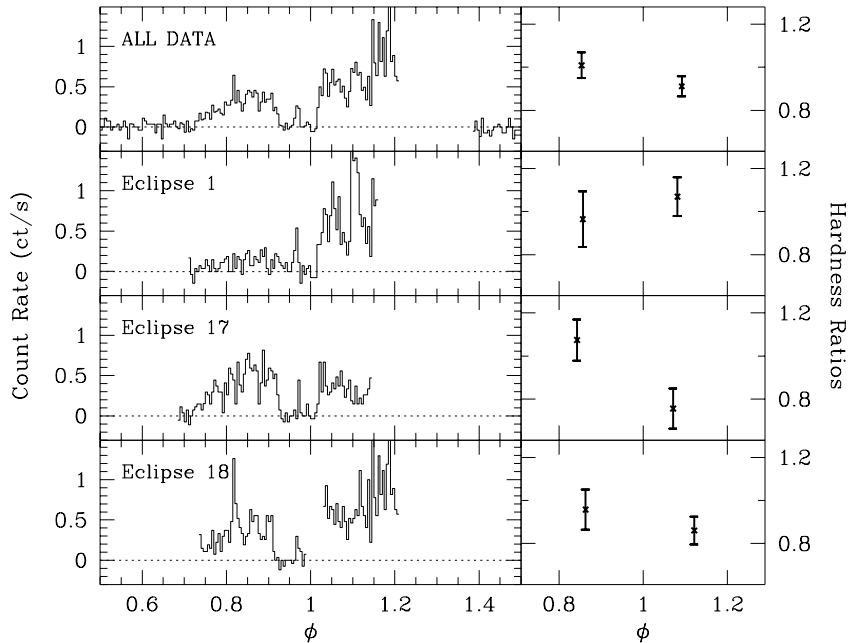


Figure 7. ROSAT light curves and hardness ratios for DP Leo.

Hardness ratios determined before and after eclipse are shown on the right side of Figure 7 for each of the ROSAT light curves. The ratio was defined as PI channels 18 through 46 (0.18 - 0.47 keV) divided by PI channels 8 through 17 (0.08 - 0.18 keV) in the 256 channel system. This definition allowed for a hardness ratio near unity for the entire observing set. The ROSAT light curves are clearly variable within a particular orbit and between orbits. The first observed eclipse showed little emission prior to the first intensity dip. The spike between the suspected position of the intensity dip and the eclipse was evident and strong variable X-ray emission was observed after eclipse. The next observed eclipse, Eclipse 17 (16 DP Leo orbits later), showed stronger emission before the intensity dip than after the eclipse. The final eclipse observation, Eclipse 18 (only one DP Leo orbit later), showed emission before the intensity dip similar to Eclipse 17, and flaring behavior after eclipse similar to Eclipse 1.

A comparison of the dearth of emission prior to eclipse in Eclipse 1 to the much stronger emission in Eclipse 17 shows that the hardness ratio likely stayed around the same or increased slightly. If the change were caused by photoelectric absorption alone, a decrease in the hardness ratio would have been expected. Data after eclipse in Eclipse 17, which shows a dearth of flares, imply a softer spectrum when compared to both data after eclipse in Eclipse 1 and data before

eclipse in Eclipse 17 where emission variations appear more active. However, inferences based upon hardness ratio variations are limited due to the paucity of observed photons.

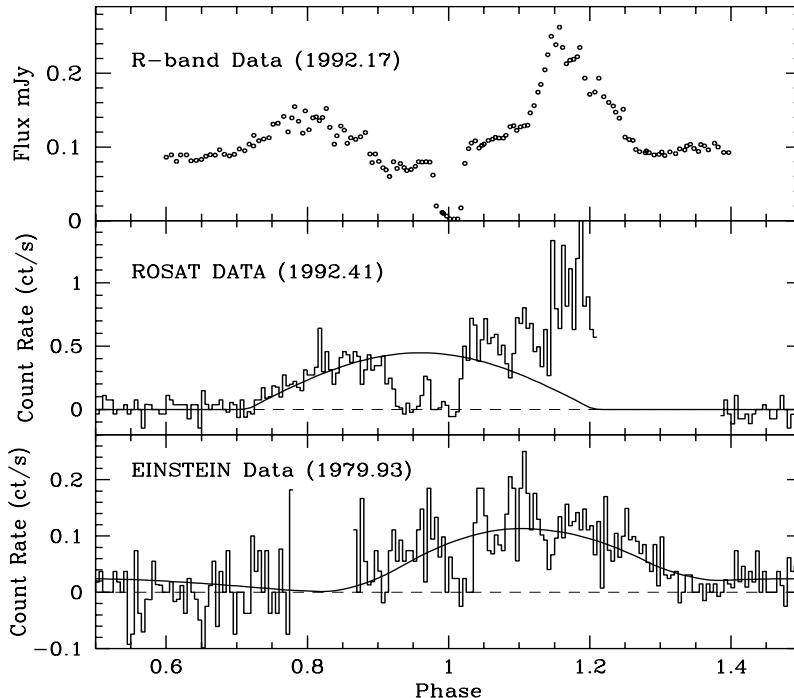


Figure 8. DP Leo light curves in R-band (from a plot by BWF), ROSAT and EINSTEIN. The dashed lines correspond to count rates of zero. The solid lines are model fits to the data.

High precision optical photometry of DP Leo taken less than three months before the PSPC observations show the center of eclipse to occur  $24 \pm 4$  seconds prior to the prediction of the Schmidt ephemeris (BWF; Bailey 1993). The duration and timing of the optical eclipse agree well with the interpretation of the second X-ray dip as originating from the eclipse by the secondary (see Figure 8).

The duration of the X-ray eclipse in DP Leo is  $3.6 \pm 0.3$  minutes with the center occurring at phase  $0.996 \pm 0.002$  phase (all phases mentioned are according to the Schmidt ephemeris) using the combined data set. Times of eclipse centers were calculated for the two observed eclipses with complete coverage. We obtained two minima timings at  $\text{HJD}2448773.21442 \pm 0.00012$  and  $\text{HJD}2448774.21235 \pm 0.00012$ . A revised ephemeris is then obtained using the above timings together with those listed by Biermann et al. (1985), Schaaf et al. (1987), Schmidt (1989), and Bailey (1993) with each timing weighted according to its associated error:

$$\begin{aligned} \text{Min.} &= \text{HJD}2444214.552934 + 0.0623628437E \\ &\quad \pm 0.000043 \pm 0.0000000007 \end{aligned}$$

The X-ray emission observed in DP Leo is assumed to be emitted as an optically thick blackbody modulated by the cosine of the viewing angle. Photometric modeling was performed on the system allowing for modulation based

upon viewing angle effects and occultation of the emission region as it rotates out of view. The geometry of the eclipse by the secondary was not included and data within the eclipse were excluded when fitting models. The initial sizes and locations of the X-ray emission regions were chosen to coincide with the cyclotron emission regions found by CW. The fluxes of these two regions as well as the sizes and positions of the regions may be fixed, constrained between limits or allowed to vary freely while the Levenberg-Marquardt method of nonlinear least-squares was used to fit the model to the observed X-ray light curves.

The EINSTEIN light curve was well fit by constraining the X-ray emission regions to the positions determined for the cyclotron emission regions. The fluxes of the emission regions were the only free parameters used to produce the model to the light curve shown in the EINSTEIN data set plot of Figure 8. The main region dominates the X-ray flux in the system from near phase 0.85 out to near phase 1.35 where the secondary emission begins to dominate. Unlike the observations with ROSAT, the level of X-ray emission is clearly above zero in EINSTEIN from phase 0.4 to near 0.55 indicating the presence of either a greatly extended main emission region or an additional second region. Optical observations from 1982 to 1989 (Biermann et al. 1985, CW) show that accretion was occurring at a second pole and supports the likelihood of two pole accretion also existing at the time of the EINSTEIN observations. Our photometric model suggests that the flux in EINSTEIN counts per unit area of the secondary accretion region is 55% of the main accretion region in X-rays observed by EINSTEIN.

The X-ray emission in 1992 from ROSAT, however, shows no evidence of X-ray emission from a second pole. The R-band photometry of BWF from 1992 (see Figure 8) was fit by BWF with a single circular emission region centered at or near the rotational meridian with a radius of 0.15 times the white dwarf's radius. The assumption of a coincident X-ray emitting region will not reproduce the observed ROSAT light curve. The data from phase 0.4 to the intensity dip were fit by a single circular emission region allowed to vary in rotational longitude, flux and size. The rotational colatitude of the spot was fixed at the BWF determination of  $100^\circ$ . The resulting model is shown in the ROSAT data set plot of Figure 8. The longitude of the spot is  $14^\circ.4$  and the spot radius is  $3^\circ.2$ . The model does not reproduce the ROSAT observations after eclipse which may be dominated by a variable rate or size of accretion blobs producing numerous flaring events. The substantial amount of emission still observed near phase 1.2 suggests that the emission may be occurring over a large region, a region with significant vertical extent or perhaps several distinct regions.

An estimate of the longitude of the X-ray emitting region may be obtained using two methods. The first method uses the intensity dip prior to the eclipse. The intensity dip lasts for a duration of  $3.8 \pm 0.3$  minutes with a center at  $0.943 \pm 0.002$  phase in the Schmidt ephemeris. Under the assumption that the intensity dip is an occultation of the X-ray emitting region by an accretion column aligned radially near the white dwarf surface, the longitude of the emitting region would be  $18^\circ.9 \pm 2^\circ.5$ .

The second method is to measure the midpoint of the bright phase emission. The bright phase is estimated to start near phase 0.72. However, the end point was not observed. If the intensity dip center corresponds to the longitude of the emitting region, then the bright phase would be expected to end near phase 1.16.

Data extend through this phase with no end to the bright phase observed before phase 1.21 and a limit to the end of the bright phase exists at 1.39 when data again resume. This implies that the longitude of the accretion region center lies between  $-20^\circ$  and  $+12^\circ$ . The allowed range is in conflict with the first method.

This conflict may be resolved in several ways. One resolution requires that X-ray absorbing matter lie along the line of sight to an X-ray emitting region positioned on the white dwarf but in a position consistent with the second method's allowed positions. Such material would be required to be stable in its relative position, in both the orbit of DP Leo and in the size of the structure, over a time period of at least one day. In addition, it must allow for less of an obscuration of the emission region just prior to the eclipse by the secondary. A possible source for such emission could be a solar-like prominence on the surface of the secondary star. Assuming the system parameters for DP Leo fit in the paper by BWF together with an emission region located at  $0^\circ$  longitude, such a region would need to extend around  $4 \times 10^4$  km, or around 0.4 times the radius of the secondary star, above the surface of the secondary.

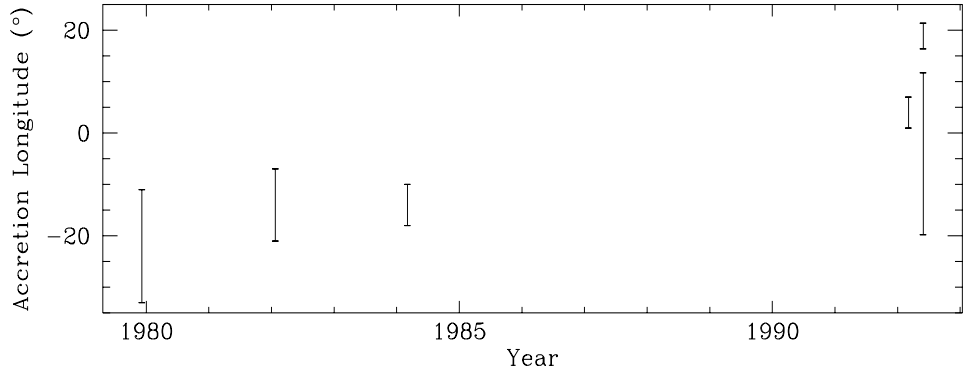


Figure 9. DP Leo accretion spot longitude positions v. time.

Another solution is for the accretion stream to be shaped to completely block the emission region at phase 0.943 and partially just prior to eclipse, yet have the emission region still close to the line of centers. A combined centered dipole and inclined quadrupole field for the white dwarf may allow for such a geometry and explain some of the observed features in DP Leo. The multipole field model of polars by Wu & Wickramasinghe (1993) provides for three magnetic poles on the surface of the white dwarf with two narrow poles lying close to the rotational axis and a band-like pole, of field strength half the axial poles, near the rotational equator. The quadrupole field of the white dwarf, which falls off by  $R^{-4}$  with distance from the white dwarf, channels the accretion stream onto the equatorial pole only near to the white dwarf (within several white dwarf radii). The accretion stream, outside of the range dominated by the quadrupole field, has a motion dictated by the momentum of the Roche lobe overflowing material and the dipole field of the white dwarf. The position of the secondary region suggests that a centered dipole, positioned so that one pole lies near the secondary region and the other  $180^\circ$  away, will tend to channel the stream ahead of the main region and out of the orbital plane. Close to the white dwarf, the quadrupolar field dominates and distorts the stream to the main accretion region. The stream, therefore, could be leading the main accretion region, as would

be necessary to produce an intensity dip at the phase observed, even though the main accretion region is near the line of centers. The distortion of the accretion stream much closer to the white dwarf, produced by the quadrupole field, may then allow for a geometry where only partial occultation of the main emission region is observed just prior to eclipse.

The variations in accretion spot longitude as a function of time are presented in Figure 9 from observations by Biermann et al. (1985), BWF and the present work. Both the ROSAT intensity dip and allowed bright phase ranges are shown. The determination of the center of the bright spot region ( $4^\circ \pm 3^\circ$ ) by BWF using their blue filter data would not appear to coincide with a similar determination using their red data (shown in Figure 8 of this paper) which would suggest a slightly larger accretion spot longitude. Evidence of an intensity dip around the phase determined with ROSAT was presented by Schaaf et al. (1987) for one out of two observations by EXOSAT from 1984. This may indicate that the geometrical shape of the absorbing material may be stable on time scales of hours to days (from ROSAT observations), variable on time scales of months (from the EXOSAT observations), yet recur after several years (between EXOSAT and ROSAT observations). However, the EXOSAT data are complicated by low counts, a high background and the flaring of nearby X-ray sources.

#### 4. Conclusions

We have determined X-ray spectral models and studied the photometric behavior from observations of TT Ari and DP Leo. TT Ari continues to show great variability in hard and soft X-rays as well as in the optical and UV. Flaring in the optical and X-ray data appear well correlated. This implies that efficient energy transfer, perhaps acoustic and magnetohydrodynamic energy transport between a disk and its corona, exist between the sources of these emissions. The relationship of the UV emission to the physical processes producing the variability at other wavelengths is currently unclear.

X-ray variability in DP Leo constrains the location of emission regions and absorbing material. X-ray observations provide a useful mechanism for the determination of variations in accretion spot positions and can, therefore, serve to test models of synchronism for the rotation of the white dwarf or movement of the magnetic field on the white dwarf. Combined dipole/multipole models of the magnetic fields in polars may be constrained in the future by determining the shape of the accretion flow close to the white dwarf surface perhaps through combined X-ray and cyclotron emission observations of high inclination systems.

Finally, recent arguments by Shu (1993) suggest that classical T Tauri systems may contain a disk similar in structure to current theories on IPs where the inner disk is disrupted by the central star's magnetic field. The wind observed in these systems is then produced in the inner portion of the remaining accretion disk. The application of some of the physical models associated with CVs may find more use in the study of the mass accreting T Tauri stars than previously believed. The reverse may also be true.

We thank M. Cropper, J. Nousek, R. Thompson and R. Wade for helpful discussions, J. Bailey for providing information on the times of minima of the

1992 optical eclipses of DP Leo prior to their publication and M. Ishida for his work and expertise on the analysis of the Ginga data.

## References

- Bailey, J. 1993, private communication
- Bailey, J., Wickramasinghe, D.T., Ferrario, L., Hough, J.H. and Cropper, M. 1993, MNRAS, 261, L31 (BWF)
- Beardmore, A.P., Ramsay, G., Osborne, J.P. et al. 1993, preprint
- Biermann, P., Schmidt, G.D., Liebert, J., Stockman, H.S., Tapia, S., Kühr, H., Strittmatter, P.A., West, S. and Lamb, D.Q. 1985, ApJ, 293, 303
- Córdova, F.A. 1993, in X-ray Binaries, W.H.G. Lewin et al. , Cambridge: Cambridge Univ., in press
- Córdova, F.A., Mason, K.O. and Nelson, J.E. 1981, ApJ, 245, 609
- Cropper, M. 1990, Space Sci.Rev., 54, 195
- Cropper, M. and Wickramasinghe, D.T. 1993, MNRAS, 260, 696 (CW)
- Frank, J, King, A.R. and Lasota, J.-P. 1988, A&A, 193, 113
- Frisch, P.C. and York, D.G. 1983, ApJ, 271, L59
- Guinan, E.F. and Sion, E.M. 1980, in The Universe at Ultraviolet Wavelengths: The First Two Years of IUE, R.D. Chapman, NASA CP2171, 477
- Hellier, C., Mason, K.O. and Mittaz, J.P.D. 1991, MNRAS, 248, 5p
- Ishida, M. 1991, Ph.D. Thesis (Univ. of Tokyo)
- Jensen, K.A., Córdova, F.A., Middleditch, J. et al. 1983, ApJ, 270, 211
- Kraft, R.P., Burrows, D.N. and Nousek, J.A. 1991, ApJ, 374, 344
- Nousek, J.A. and Lesser, A. 1993, ROSAT Newsletter 8, 13
- Ramsay, G., Rosen, S.R., Mason, K.O., Cropper, M.S., and Watson, M.G. 1993, MNRAS, 262, 993
- Robinson, C.R., Córdova, F.A. and Ishida, M. 1993, in preparation
- Schmidt, G.D. 1988, in Polarized Radiation of Circumstellar Origin, G.V. Coyne et al. , Vatican: Vatican Obs., 85
- Schaaf, R., Pietsch, W. and Biermann, P. 1987, A&A, 174, 357
- Semeniuk, I., Schwarzenberg-Czerny, A., Duerbeck, H. et al. 1987, Acta Astron., 37, 197
- Shafter, A.W., Szkody, P., Liebert, J. et al. 1985, ApJ, 290, 707
- Shu, F. 1993, preprint.
- Thorstensen, J.R., Smak, J. and Hessman, F.V. 1985, PASP, 97, 437
- Tremko, J. 1992, Inf. Bull. Var. Stars 3763
- Turner, T.J. and George, I.M. 1993, ROSAT PSPC Calibration Guide
- Voikhanskaya, N.F. 1990, Astrofizik. Issledovanija - Sofia, 30, 3 (translated in Bull. Spec. Astrophys. Obs. - N. Caucasus, 30,1)
- Wu, K. and Wickramasinghe, D.T. 1993, MNRAS, 260, 141
- Young and Schneider 1981, ApJ, 247, 960